RFOD: Random Forest-based Outlier Detection for Tabular Data

Yihao Ang
National University of Singapore
yihao_ang@comp.nus.edu.sg

Peicheng Yao
National University of Singapore
peicheng.yao@u.nus.edu

Yifan Bao
National University of Singapore
yifan_bao@comp.nus.edu.sg

Yushuo Feng*
Huazhong University of Science &
Technology
u202315134@hust.edu.cn

Qiang Huang
Harbin Institute of Technology
(Shenzhen)
huangqiang@hit.edu.cn

Anthony K. H. Tung
National University of Singapore
atung@comp.nus.edu.sg

Zhiyong Huang
National University of Singapore
huangzy@comp.nus.edu.sg

ABSTRACT

Outlier detection in tabular data is crucial for safeguarding data integrity in high-stakes domains such as cybersecurity, financial fraud detection, and healthcare, where anomalies can cause serious operational and economic impacts. Despite advances in both data mining and deep learning, many existing methods struggle with mixed-type tabular data, often relying on encoding schemes that lose important semantic information. Moreover, they frequently lack interpretability, offering little insight into which specific values cause anomalies. To overcome these challenges, we introduce **RFOD**, a novel **R**andom **F**orest-based **O**utlier **D**etection framework tailored for tabular data. Rather than modeling a global joint distribution, RFOD reframes anomaly detection as a feature-wise conditional reconstruction problem, training dedicated random forests for each feature conditioned on the others. This design robustly handles heterogeneous data types while preserving the semantic integrity of categorical features. To further enable precise and interpretable detection, RFOD combines Adjusted Gower's Distance (AGD) for cell-level scoring, which adapts to skewed numerical data and accounts for categorical confidence, with Uncertainty-Weighted Averaging (UWA) to aggregate cell-level scores into robust row-level anomaly scores. Extensive experiments on 15 real-world datasets demonstrate that RFOD consistently outperforms state-of-the-art baselines in detection accuracy while offering superior robustness, scalability, and interpretability for mixed-type tabular data.

1 INTRODUCTION

Outliers, data instances whose feature combinations significantly deviate from the dominant distribution, pose substantial challenges for data-driven decision-making [2]. Undetected anomalies can distort analyses, conceal critical insights, and disrupt operations. These risks are particularly acute in high-stakes domains such as cybersecurity [34, 35], financial fraud detection [15, 48], healthcare [13, 45], and industrial monitoring [6, 7, 10], where timely and interpretable anomaly detection is essential for ensuring reliability and economic viability.

In tabular data, effective outlier detection approaches require satisfying two interlinked goals: (1) accurately identify anomalous instances, and (2) pinpoint the specific feature values responsible for the anomalies. Achieving both objectives is crucial not only for high detection performance but also for providing interpretable and actionable insights necessary in real-world applications. Despite extensive research [2, 9, 11, 21, 25, 27, 28, 30, 36, 39, 40, 50, 55], outlier detection on tabular data remains particularly challenging. Unlike homogeneous data types such as images or text, tabular datasets often consist of mixed numerical and categorical features with diverse distributions and complex interdependencies [5, 8, 18, 24]. Moreover, anomalies frequently affect only specific cells within a row, rendering purely row-level methods insufficient for precise localization [3].

Vanilla data mining approaches, such as Local Outlier Factor (LOF) [12], Isolation Forest (IF) [31], One-Class Support Vector Machines (OCSVM) [51], Empirical Cumulative Distribution (ECOD) [29], and OutlierTree (OT) [18], typically rely on global proximity or statistical heuristics. While efficient and easy to implement, they often treat features independently and fail to capture the subtle multivariate relationships critical for detecting contextual anomalies. In contrast, modern deep learning methods, including Deep Support Vector Data Description (Deep SVDD) [42], Deviation Networks (DevNet) [38], Internal Contrastive Learning (ICL) [43], Scale Learning-based deep Anomaly Detection (SLAD) [53], and Deep Isolation Forest (DIF) [52], attempt to learn complex dependencies through latent representations. Nevertheless, these approaches predominantly assume purely numerical inputs and suffer from two critical limitations: (1) they are not natively designed for *mixed-type* data and rely on preprocessing (e.g., one-hot encoding) that
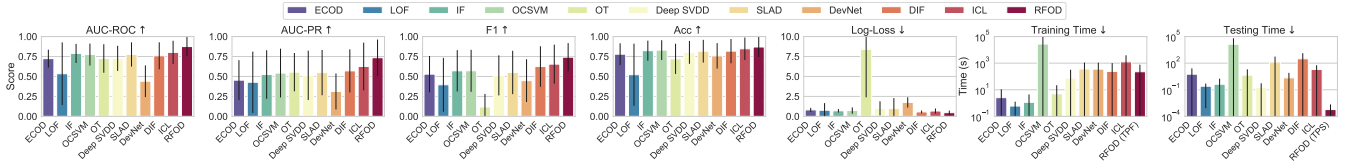
Figure 1: Average anomaly detection performance of all methods across 15 real-world tabular datasets. RFOD consistently ranks at or near the top, demonstrating strong accuracy and robustness over both data mining and deep learning baselines.

may lose semantic nuance, and (2) their *black-box* nature impedes interpretability, making it difficult to trace the rationale behind anomaly scores.

Figure 1 from our experiments highlights these challenges. While some deep learning methods occasionally excel on specific datasets, their performance is inconsistent, particularly for mixed-type data. Traditional data mining methods, though faster and more interpretable, often lag in detection accuracy and fine-grained insights. No existing method consistently delivers strong performance across the diverse landscape of tabular data.

To bridge this gap, we introduce **RFOD**, a novel **R**andom **F**orest-based **O**utlier **D**etection framework specifically designed for tabular data. Unlike conventional methods that model the joint distribution of all features, RFOD reframes anomaly detection as a **feature-wise conditional reconstruction** problem. It trains dedicated random forests for each feature, conditioned on the remaining features, enabling nuanced modeling of inter-feature dependencies and flexible adaptation to heterogeneous data types. During inference, RFOD reconstructs each feature value for test instances, quantifies deviations via residuals, adjusts anomaly scores based on model uncertainty, and aggregates these signals into robust row-level anomaly scores. RFOD distinguishes itself from existing methods through several key innovations, each designed to address the challenges of mixed-type tabular data:

- **Feature-Specific Random Forests:** Independently trained forests for each feature capture localized conditional relationships, bypassing restrictive global assumptions and enabling precise localization of anomaly signals, particularly when anomalies affect only a subset of features.
- **Forest Pruning:** A principled mechanism using out-of-bag (OOB) validation to retain only the most informative decision trees in each forest, reducing noise and improving both generalization and computational efficiency.
- **Adjusted Gower's Distance (AGD):** We introduce AGD for fine-grained, cell-level anomaly measurement. Unlike traditional distance metrics, AGD adapts to skewed numerical distributions via quantile normalization and incorporates confidence-weighted matching for categorical features, yielding robust, interpretable cell-level anomaly scores.
- **Uncertainty-Weighted Averaging (UWA):** RFOD aggregates cell-level anomaly scores into row-level scores through UWA, dynamically weighting cell contributions based on prediction confidence. This mechanism prevents noisy or uncertain predictions from diluting the overall anomaly signal.

Our comprehensive experiments across 15 real-world tabular datasets demonstrate RFOD's substantial empirical advantages. As shown in Figure 1, RFOD consistently achieves the highest average anomaly detection performance across all key metrics, including AUC-ROC, AUC-PR, F1, Accuracy, and Log-Loss, surpassing ten state-of-the-art baselines spanning both data mining and deep learning paradigms. Remarkably, RFOD delivers up to a 9.1% gain in AUC-ROC over the best competing method and achieves an average 91.2% reduction in test-time latency, compared to leading alternatives, underscoring its scalability and practical value. Ablation studies confirm the critical roles played by RFOD's components, while detailed case analyses demonstrate how RFOD provides actionable, transparent explanations by pinpointing anomalies at both the cell and row levels. Together, these results position RFOD as a robust, interpretable, and scalable solution for outlier detection in tabular data, effectively addressing longstanding gaps in handling mixed-type datasets and delivering insights vital for real-world decision-making.

The remainder of this paper is structured as follows: Section 2 reviews related work; Section 3 formulates the problem; Section 4 details the RFOD framework; Section 5 presents extensive experimental results and analyses; and Section 6 concludes the paper.

2 RELATED WORK

Outlier detection for tabular data has long been a central topic in data mining and machine learning. Existing research broadly falls into two categories: (1) data mining–based methods and (2) deep learning–based approaches. We review each and position our proposed RFOD framework within this landscape.

2.1 Data Mining-based Outlier Detection

Traditional data mining methods detect anomalies by measuring deviations from expected patterns using statistical, density-based, or proximity-based criteria. These approaches often rely on hand-crafted features, pairwise distances, or tree-based models to quantify abnormality [17]. A seminal method in this category is IF [31], which isolates outliers through recursive random partitioning, using the average path length of instances in trees as an indicator of anomaly. Similarly, LOF [12] assesses how much a data point deviates from the local density of its neighbors, making it effective in heterogeneous density settings. OCSVM [51] models the decision boundary around normal data in feature space, treating points outside this boundary as anomalies. More recently, ECOD [29] proposes a nonparametric approach to estimate anomaly scores directly from empirical distributions, focusing on tail probabilities to capture rare events. Tree-based methods have also emerged for interpretable detection. OT [18] constructs decision trees that model each feature as a function of others, flagging data points that deviate significantly from expected branches.

Despite their efficiency and interpretability, these methods often suffer from three key limitations: (1) They usually assume independent feature contributions, overlooking multivariate interactions

critical for detecting contextual anomalies. (2) Many struggle to handle mixed-type data without resorting to potentially lossy encoding schemes. (3) Their ability to pinpoint cell-level anomalies is limited, hindering detailed diagnostics. RFOD advances this line of research by leveraging Random Forests in a feature-wise conditional reconstruction paradigm. This design offers three advantages: (1) native support for mixed-type data, eliminating the need for encoding schemes that risk losing feature semantics; (2) enhanced interpretability through tree-based inference paths, enabling clear attribution of anomalies to specific features and values; and (3) robustness and generalization, achieved through ensemble averaging and refined further by selective tree pruning, which removes noisy or redundant predictors.

2.2 Deep-Learning-based Outlier Detection

The rise of deep learning has fueled a new generation of outlier detection methods that automatically learn complex representations from raw data [16]. These approaches have achieved impressive results, particularly in high-dimensional or structured domains like images and text. For instance, Deep SVDD [42] extends traditional Support Vector Data Description (SVDD) [49] by learning a hypersphere in a latent space to enclose normal samples, flagging deviations as anomalies. DevNet [38] introduces a semi-supervised framework that explicitly models deviations between known anomalies and normal instances, improving detection under limited anomaly labels. ICL [43] leverages self-supervised contrastive signals to distinguish anomalies by emphasizing internal dissimilarities in learned representations. More recently, SLAD [53] focuses on learning scale-sensitive transformations, uncovering subtle patterns indicative of anomalies. Hybrid approaches have also gained research attention. DIF [52] augments traditional IF with neural embeddings to combine expressive power with tree-based interpretability.

However, deep learning–based techniques face significant limitations when applied to tabular data. First, most models are designed for numerical inputs and struggle with categorical features, requiring preprocessing (e.g., one-hot encoding or learned embeddings) that can inflate dimensionality or obscure semantic meaning [24]. Second, neural networks often operate as black boxes, offering limited insight into which features drive anomaly decisions, a critical drawback in domains where explanations are mandatory for trust and compliance [29]. RFOD bridges these gaps by integrating the strengths of tree-based approaches with a novel feature-wise reconstruction strategy. Its design handles mixed-type data seamlessly without complex embeddings and offers principled mechanisms like Adjusted Gower's Distance (AGD) and Uncertainty-Weighted Averaging (UWA) to enhance robustness and interoperability, addressing longstanding challenges in tabular anomaly detection.

3 PROBLEM FORMULATION

Let $X_{\text{train}} \in \mathbb{R}^{n \times d}$ be a training set with n samples (rows) and d features (columns), and $X_{\text{test}} \in \mathbb{R}^{m \times d}$ be a test set with m samples. We denote the i-th sample as $x_i = [x_{i,1}, \cdots, x_{i,d}]$, the j-th feature as $x^j = [x_{1,j}, \cdots, x_{n,j}]$, and the individual cell as $x_{i,j}$. The objective of outlier detection is to quantify how anomalous each test sample $x_i \in X_{\text{test}}$ is, by computing an anomaly score. To support both

Table 1: Frequently used notations.

Symbol	Description
$X_{\text{train}} \in \mathbb{R}^{n \times d}$	Training set with n samples and d features: $X_{\text{train}} = [x_{i,j}]$
$x_i \in \mathbb{R}^d$	i-th sample: $x_i = [x_{i,1}, \cdots, x_{i,d}]$
$x^j \in \mathbb{R}^n$	j-th feature: $x^j = [x_{1,j}, \cdots, x_{n,j}]$
RF_j	Random Forest trained for feature x^j
β	Retaining ratio for forest pruning
$X_{\text{test}} \in \mathbb{R}^{m \times d}$	Test set with m samples and d features: $X_{\text{test}} = [x_{i,j}]$
$\hat{X}_{\text{test}} \in \mathbb{R}^{m \times d}$	Reconstructed test set: $\hat{X}_{\text{test}} = [\hat{x}_{i,j}]$
$AGD^{(\text{num})}(x_{i,j}, \hat{x}_{i,j})$	Adjusted Gower's Distance (AGD) for numerical features
$AGD^{(\text{cat})}(x_{i,j}, \hat{x}_{i,j})$	Adjusted Gower's Distance (AGD) for categorical features
α	Quantile parameter for AGD for numerical features
$S_{\text{cell}} \in \mathbb{R}^{m \times d}$	Cell-level anomaly scores: $S_{\text{cell}} = [s_{i,j}]$
$U \in \mathbb{R}^{m \times d}$	Uncertainty matrix: $U = [u_{i,j}]$
$W \in \mathbb{R}^{m \times d}$	Confidence weights: $W = [w_{i,j}]$
$s_{\text{row}} \in \mathbb{R}^m$	Row-level anomaly scores: $s_{\text{row}} = [s_{\text{row},1}, \cdots, s_{\text{row},m}]$

fine-grained analysis and robust detection, we adopt a two-stage scoring approach: first assigning cell-level anomaly scores, then aggregating them into row-level scores.

Definition 3.1 (Outlier Detection): *Given a test set $X_{test} = [x_{i,j}] \in \mathbb{R}^{m \times d}$, the goal is to compute a cell-level anomaly score $s_{i,j}$ for each feature value $x_{i,j}$, producing a cell-level anomaly matrix:*

$$S_{cell} = [s_{i,j}] \in \mathbb{R}^{m \times d}.$$

The anomaly score for row x_i is then computed via an aggregation function $g : \mathbb{R}^d \to \mathbb{R}$, as follows:

$$s_{row,i} = g(s_i) = g([s_{i,1}, \cdots, s_{i,d}]),$$

yielding a row-level anomaly score vector:

$$s_{row} = [s_{row,1}, \cdots, s_{row,m}] \in \mathbb{R}^m.$$

*Higher values of $s_{row,i}$ indicate greater likelihoods that x_i is an outlier.*

This hierarchical formulation supports both detection accuracy and interpretability: cell-level scores reveal which features contribute to an anomaly, while row-level scores provide a global ranking. We adopt this structure throughout the paper. A summary of frequently used notations is provided in Table 1.

4 RFOD FRAMEWORK

We present RFOD, a robust and interpretable framework for detecting anomalies in tabular data. Unlike traditional approaches that model a global joint distribution, often brittle in heterogeneous or high-dimensional settings, RFOD reframes anomaly detection as a **feature-wise conditional reconstruction** problem. It learns how each feature behaves when conditioned on the others, enabling flexible, scalable, and context-aware anomaly detection.

Given a training set $X_{\text{train}} \in \mathbb{R}^{n \times d}$ with n samples and d features, RFOD performs a leave-one-feature-out decomposition. For each feature x^j ($1 \leq j \leq d$), it builds a dedicated random forest RF_j that treats x^j as the target and uses the remaining $(d-1)$ features as inputs. This results in d independent forests $\{RF_1, \cdots, RF_d\}$, each capturing conditional patterns specific to a feature. These forests are trained in parallel for efficiency.
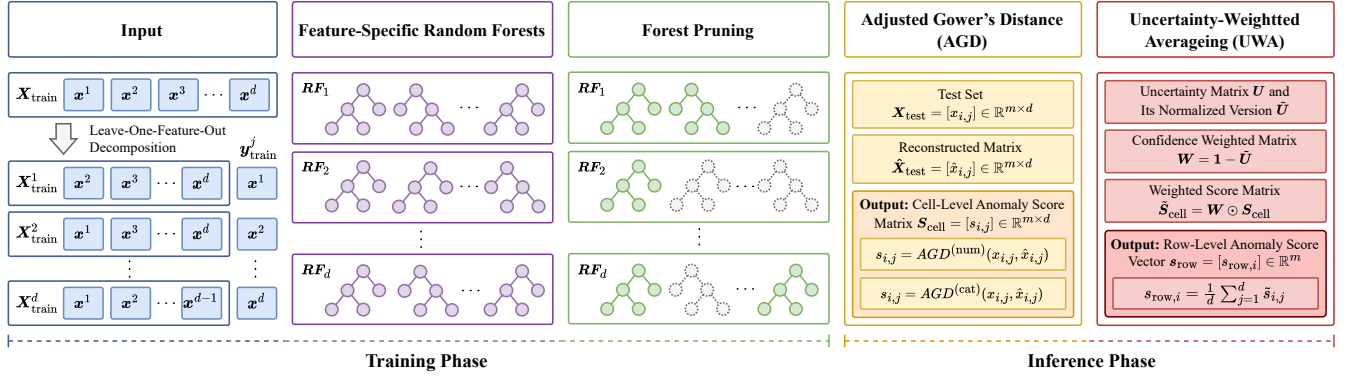
Figure 2: Overview of RFOD. Given training data $X_{\text{train}} \in \mathbb{R}^{n \times d}$, RFOD applies a leave-one-feature-out strategy, training a dedicated forest RF_j for each feature x^j using the remaining features. Each forest is pruned via out-of-bag (OOB) validation to enhance generalization. At inference, the pruned forests reconstruct X_{test} to form $\hat{X}_{\text{test}}$, which is compared against X_{test} using Adjusted Gower's Distance (AGD) to compute cell-level anomaly scores S_{cell}. These are aggregated into row-level scores s_{row} via Uncertainty-Weighted Averaging (UWA) for interpretable and robust detection.

During inference, each test sample $x_i = [x_{i,1}, \cdots, x_{i,d}]$ from $X_{\text{test}} \in \mathbb{R}^{m \times d}$ is evaluated by the d trained forests. For each feature $x_{i,j}$, the corresponding forest RF_j predicts a value $\hat{x}_{i,j}$ based on the remaining features. In normal cases, $\hat{x}_{i,j}$ should closely match $x_{i,j}$, reflecting consistency with learned patterns. In contrast, anomalies often exhibit larger deviations between $x_{i,j}$ and $\hat{x}_{i,j}$, resulting in higher residuals and anomaly scores. Notably, even when $\hat{x}_{i,j}$ appears accurate, inconsistencies in decision paths, such as diverging leaf nodes across trees, may signal contextual anomalies. This enables RFOD to capture overt and subtle deviations from normality.

As illustrated in Figure 2, RFOD comprises four key modules:

(1) **Feature-Specific Random Forests (§4.1)**: Train a separate forest for each feature, using the others as input, to learn conditional distributions.

(2) **Forest Pruning (§4.2)**: Retain only the most informative trees using out-of-bag (OOB) validation, controlled by a retaining ratio β.

(3) **Adjusted Gower's Distance (AGD) (§4.3)**: Compare actual and predicted values using AGD to produce a cell-level anomaly score matrix.

(4) **Uncertainty-Weighted Averaging (UWA) (§4.4)**: Use tree disagreement to estimate uncertainty, which weights cell scores when aggregating to row-level scores.

This architecture enables robust, interpretable, and scalable anomaly detection across diverse tabular domains.

4.1 Feature-Specific Random Forests

To capture complex inter-feature dependencies, RFOD employs a leave-one-feature-out decomposition strategy. Instead of fitting a single global model across all features, it constructs a set of feature-specific random forests, each dedicated to learning the conditional behavior of one feature given the rest.

Leave-One-Feature-Out Decomposition. For each feature x^j ($1 \leq j \leq d$) in the training set $X_{\text{train}} \in \mathbb{R}^{n \times d}$, RFOD treats x^j as the target and uses the remaining $(d-1)$ features as predictors. This results in d overlapping sub-training sets of the form $(X_{\text{train}}^j, y_{\text{train}}^j)$, where $X_{\text{train}}^j = X_{\text{train}} \setminus \{x^j\}$ and $y_{\text{train}}^j = x^j$. Each sub-training set

is used to train a dedicated Random Forest RF_j that approximates the conditional distribution of the target feature:

$$RF_j : X_{\text{train}}^j \in \mathbb{R}^{n \times (d-1)} \rightarrow y_{\text{train}}^j \in \mathbb{R}^n. \tag{1}$$

The model type is selected based on the target feature's data type: Random Forest classifiers are used for categorical features and regressors for numerical ones (see Lines 5–8 in Algorithm 1). Each RF_j learns the typical behavior of its feature under normal conditions, conditioned on the context of other features. Together, the d forests encode the feature-wise conditional distributions that define the structure of normal data.

Remarks. This design offers three key advantages: (1) By modeling each feature conditionally, RFOD captures both global and local inter-feature dependencies, enabling the detection of subtle context-specific anomalies. (2) Avoiding full joint modeling mitigates the curse of dimensionality, which often hinders anomaly detection in high-dimensional spaces [54]. (3) The independent training of each forest allows for straightforward parallelization, significantly improving efficiency–a benefit we empirically validate in **§5.6**.

4.2 Forest Pruning

Motivation. Although Random Forests are known for their robustness, they often include a large number of decision trees, many of which contribute little to predictive accuracy. These low-quality or redundant trees not only increase memory and inference costs but can also introduce noise that undermines generalization. To mitigate these issues, RFOD integrates a pruning module that selectively retains the most informative trees from each feature-specific forest, thereby enhancing both efficiency and model robustness.

Pruning Strategy. Given a feature-specific forest $RF = \{T_1, \cdots, T_t\}$ with t decision trees, RFOD applies a pruning strategy that leverages out-of-bag (OOB) validation–a built-in mechanism of Random Forests. Each tree T_i ($1 \leq i \leq t$) is evaluated on its OOB samples using either AUC-ROC (for classification tasks) or the coefficient of determination R^2 (for regression tasks). Formally, the OOB score
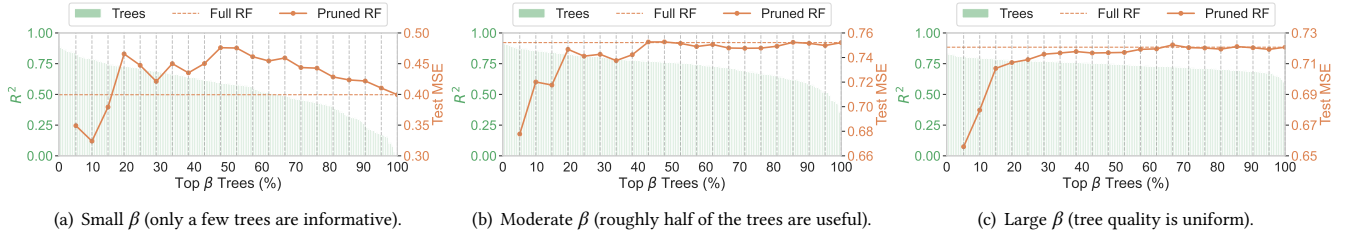
(a) Small β (only a few trees are informative). (b) Moderate β (roughly half of the trees are useful). (c) Large β (tree quality is uniform).

Figure 3: Illustration of forest pruning with varying retaining ratio β.

$\phi(T_i)$ is computed as:

$$\phi(T_i) = \begin{cases} \text{AUC-ROC}(T_i), & \text{for classification} \\ R^2(T_i). & \text{for regression} \end{cases}$$

The trees are sorted in descending order of $\phi(T_i)$, yielding an index permutation $U(1), \cdots, U(t)$ such that $\phi(T_{U(1)}) \geq \cdots \geq \phi(T_{U(t)})$. The top $\lfloor \beta \cdot t \rfloor$ trees are retained:

$$\text{Prune}(\boldsymbol{RF}) = \left\{ T_{U(i)} \mid 1 \leq i \leq \lfloor \beta \cdot t \rfloor \right\},$$

where $\beta \in (0, 1]$ is the retaining ratio (see Line 9 in Algorithm 1).

This pruning procedure compresses the model and reduces inference overhead without sacrificing–and often improving–detection performance. As shown in the ablation study (**§5.4**), carefully pruned forests frequently outperform their unpruned counterparts, particularly in high-dimensional settings.

Example 4.1: Figure 3 illustrates the effect of varying the pruning ratio $\beta \in [5\%, 100\%]$ (in 5% increments) on model performance across three representative numerical prediction tasks. For each task, decision trees are ranked by their out-of-bag (OOB) R^2 scores, and subsets comprising the top-ranked trees are retained. In each subfigure, green bars (left y-axis) indicate the R^2 of individual trees. The orange solid curve (right y-axis) shows the test MSE of the pruned forest as β increases, while the dashed orange line denotes the baseline test MSE of the full (unpruned) forest.

- **Small β** (Figure 3(a)): When only a few trees are informative, retaining the top 20% reduces test MSE by about 16.6%. Including more low-quality trees leads to performance degradation.
- **Moderate β** (Figure 3(b)): When roughly half of the trees are useful, performance stabilizes around $\beta = 0.5$, achieving a favorable trade-off between model size and accuracy.
- **Large β** (Figure 3(c)): When tree quality is relatively uniform, pruning yields marginal gains. Nevertheless, using a moderately high β (e.g., 0.8) still reduces model size without sacrificing accuracy.

In summary, this adaptive pruning strategy aligns with the underlying distribution of tree quality–pruning aggressively when the ensemble is noisy and conservatively when tree quality is consistent. This flexibility enables RFOD to maintain robust performance while improving efficiency. △

4.3 Adjusted Gower's Distance

After forest pruning, the model predicts each entry of the test set $X_{\text{test}} = [x_{i,j}] \in \mathbb{R}^{m \times d}$, producing the reconstruction matrix $\hat{X}_{\text{test}} = [\hat{x}_{i,j}] \in \mathbb{R}^{m \times d}$. Each predicted value $\hat{x}_{i,j}$ estimates the actual cell $x_{i,j}$ based on conditional patterns learned from normal data. To identify anomalies, RFOD computes a fine-grained anomaly score matrix $S_{\text{cell}} = [s_{i,j}] \in \mathbb{R}^{m \times d}$ by comparing each actual value to its prediction. Each score $s_{i,j}$ reflects the degree of deviation for a single feature, offering interpretability at the cell level.

Gower's Distance (GD) and Its Limitations. A key challenge is choosing a distance metric suitable for mixed-type tabular data. Traditional metrics like Euclidean or cosine distance assume homogeneous feature types and overlook prediction uncertainty. Gower's Distance (GD) [22] is more appropriate, as it handles both numerical and categorical features:

- For **numerical features**, it employs min-max normalization:

$$GD^{(\text{num})}(x_{i,j}, \hat{x}_{i,j}) = \frac{|x_{i,j} - \hat{x}_{i,j}|}{\max(\boldsymbol{x}^j) - \min(\boldsymbol{x}^j)},$$

  while the IQR-based variant [20] improves robustness by replacing the denominator with the interquartile range:

$$GD_{\text{IQR}}^{(\text{num})}(x_{i,j}, \hat{x}_{i,j}) = \frac{|x_{i,j} - \hat{x}_{i,j}|}{Q_{0.75}(\boldsymbol{x}^j) - Q_{0.25}(\boldsymbol{x}^j)},$$

  where $Q_{0.25}$ and $Q_{0.75}$ are the 25- and 75-quantiles of feature $\boldsymbol{x}^j$, respectively.

- For **categorical features**, GD is defined by binary matching:

$$GD^{(\text{cat})}(x_{i,j}, \hat{x}_{i,j}) = \begin{cases} 0, & \text{if } x_{i,j} = \hat{x}_{i,j} \\ 1. & \text{otherwise} \end{cases}$$
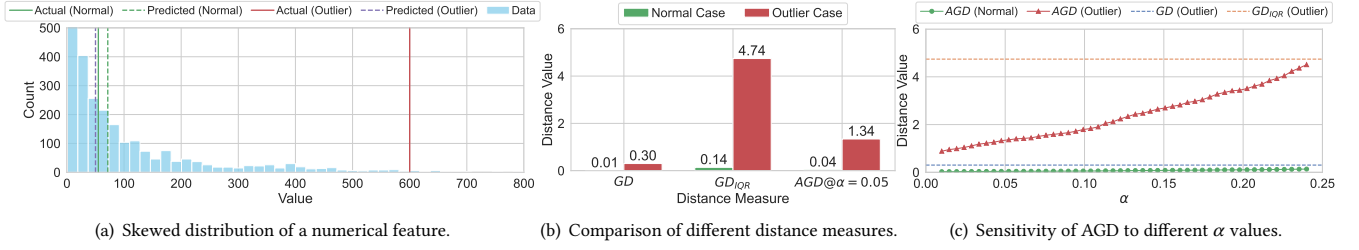
The final distance is the average of these per-feature scores.

Despite its widespread use, GD suffers from two key limitations. First, for numerical features, standard scaling methods such as minmax and IQR are sensitive to skewed or heavy-tailed distributions, which can distort the computed dissimilarities. Second, for categorical features, GD relies on binary matching, disregarding model confidence and thereby failing to differentiate between confident and uncertain predictions.

Adjusted Gower's Distance (AGD). To address these issues, we propose Adjusted Gower's Distance (AGD), a metric tailored for anomaly detection in tabular data. It incorporates:

- **α-Quantile Scaling:** A generalization of IQR scaling for numerical features that adapts to distributional asymmetry.
- **Confidence-Aware Scoring:** A soft matching scheme for categorical features based on class probability.

This formulation yields robust and interpretable scores even under skewed distributions and prediction uncertainty. Definitions for numerical and categorical features are given below.

(a) Skewed distribution of a numerical feature.   (b) Comparison of different distance measures.   (c) Sensitivity of AGD to different α values.

Figure 4: Challenges of existing Gower's Distance (GD) and the proposed AGD for numerical features.

Definition 4.1 (AGD for Numerical Features): *For numerical features, AGD is defined via adaptive α-quantile scaling:*

$$AGD^{(num)}(x_{i,j}, \hat{x}_{i,j}) = \frac{|x_{i,j} - \hat{x}_{i,j}|}{Q_{1-\alpha}(\boldsymbol{x}^j) - Q_{\alpha}(\boldsymbol{x}^j)}, \qquad (2)$$

where $\alpha \in (0, 0.5)$ controls sensitivity to distribution tails; Q_α and $Q_{1-\alpha}$ are the α- and $(1-\alpha)$-quantiles of feature $\boldsymbol{x}^j$, respectively.

Example 4.2 (AGD for Numerical Features): Figure 4 illustrates the behavior of Adjusted Gower's Distance (AGD) on a skewed numerical feature from the Pageblocks dataset [32]. In Figure 4(a), we show the feature's value distribution, highlighting actual and predicted values for both a normal and an outlier instance. For the normal case, the predicted value (green dashed line) closely aligns with the actual value (green solid line), indicating consistency with learned patterns. In contrast, the outlier's prediction (purple dashed line) substantially deviates from its actual value (red solid line), reflecting an anomalous behavior.

Figure 4(b) compares the distance values computed by traditional GD, IQR-based GD, and AGD (with $\alpha = 0.05$). Traditional GD underestimates the anomaly score (0.30), while the IQR-based variant overshoots with an inflated value (4.74). AGD provides a more balanced assessment, assigning a low score (0.04) to the normal instance and a higher, yet reasonable, score (1.34) to the outlier.

Lastly, Figure 4(c) visualizes how the choice of α influences AGD's sensitivity. Smaller α values yield behavior similar to traditional GD, while larger values resemble IQR-based scoring. A comprehensive sensitivity analysis is provided in §5.7. △

Definition 4.2 (AGD for Categorical Features): *For categorical features, AGD transforms binary matching into prediction confidence:*

$$AGD^{(cat)}(\boldsymbol{x}_{i,j}, \hat{x}_{i,j}) = 1 - p_{x_{i,j}}, \qquad (3)$$

where $p_{x_{i,j}}$ is the predicted probability of the true category $x_{i,j}$. This formulation reflects not only correctness but also model certainty.

Example 4.3 (AGD for Categorical Features): Table 2 illustrates how AGD captures prediction confidence for categorical features. For correct predictions (Rows 1, 2, and 4), GD assigns a fixed score of 0, ignoring confidence levels. In contrast, AGD reflects varying certainty by assigning lower scores to more confident predictions. For misclassifications (Rows 3, 5, and 6), GD gives a score of 1 regardless of prediction quality, whereas AGD varies the score based on the confidence of the incorrect prediction. △

Cell-Level Scoring. Finally, to compute cell-level anomaly scores, RFOD applies AGD between the original test matrix $X_{\text{test}} = [x_{i,j}]$ and its reconstructed counterpart $\hat{X}_{\text{test}} = [\hat{x}_{i,j}]$. This yields the

Table 2: Illustrative examples of probability-based adjustments in AGD for categorical features, highlighting how model confidence influences dissimilarity scoring.

$x_{i,j}$	$\hat{x}_{i,j}$	Predicted Probability	$GD^{(cat)}(x_{i,j}, \hat{x}_{i,j})$	$AGD^{(cat)}(x_{i,j}, \hat{x}_{i,j})$
A	A	$p_A = 0.8, p_B = 0.2$	0	$1 - 0.8 = 0.2$
A	A	$p_A = 0.6, p_B = 0.4$	0	$1 - 0.6 = 0.4$
A	B	$p_A = 0.3, p_B = 0.7$	1	$1 - 0.3 = 0.7$
A	A	$p_A = 0.5, p_B = 0.3, p_C = 0.2$	0	$1 - 0.5 = 0.5$
A	C	$p_A = 0.1, p_B = 0.2, p_C = 0.7$	1	$1 - 0.1 = 0.9$
A	B	$p_A = 0.2, p_B = 0.7, p_C = 0.1$	1	$1 - 0.2 = 0.8$

complete cell-level anomaly score matrix $S_{\text{cell}} = [s_{i,j}] \in \mathbb{R}^{m \times d}$, where each score is defined as:

$$s_{i,j} = \begin{cases} AGD^{(num)}(x_{i,j}, \hat{x}_{i,j}), & \text{if } x_{i,j} \text{ is numerical} \\ AGD^{(cat)}(x_{i,j}, \hat{x}_{i,j}). & \text{if } x_{i,j} \text{ is categorical} \end{cases}$$

High anomaly scores indicate feature values that deviate significantly from their expected behavior, allowing RFOD to pinpoint not only anomalous rows but also the exact cells responsible. This fine-grained interpretability is critical for tasks like root cause analysis and transparent anomaly attribution [6, 29, 47].

4.4 Uncertainty-Weighted Averaging

Unweighted Averaging. While cell-level anomaly scores provide fine-grained interpretability, many real-world applications require a single anomaly score per row [17, 29, 52]. A simple approach is to average the cell-level scores across each row without weighting. Yet, this naive method assumes equal reliability across all features, which is often unrealistic in heterogeneous tabular data. As a result, noisy or uncertain predictions may distort the row-level score, either inflating noise or masking true anomalies.

Uncertainty-Weighted Averaging (UWA). To address this, we propose Uncertainty-Weighted Averaging (UWA), an adaptive aggregation scheme that adjusts each cell's influence based on the model's predictive confidence. Leveraging the ensemble structure of Random Forests, we quantify uncertainty as the standard deviation (STD) of predictions across decision trees: higher STDs indicate greater uncertainty and result in lower weights, while lower STDs imply confidence and are upweighted accordingly.

As described in Algorithm 1 (Lines 13–16), we first compute an uncertainty matrix $U = [u_{i,j}] \in \mathbb{R}^{m \times d}$, where each $u_{i,j}$ denotes the STD of predictions for $\hat{x}_{i,j}$. Each row $\boldsymbol{u}_i$ is then normalized to yield

a row-wise uncertainty profile:

$$\tilde{\boldsymbol{u}}_i = \frac{\boldsymbol{u}_i}{\sum_{j=1}^{d} u_{i,j}}, \ \forall i \in \{1, \cdots, m\}.$$

The resulting matrix $\tilde{U} = [\tilde{\boldsymbol{u}}_1, \cdots, \tilde{\boldsymbol{u}}_m]$ is subtracted from an all-one matrix to produce the confidence weight matrix $W \in \mathbb{R}^{m \times d}$:

$$W = \mathbf{1}^{m \times d} - \tilde{U}.$$

Lower uncertainty leads to higher confidence weights. Next, given $S_{\text{cell}} = [s_{i,j}] \in \mathbb{R}^{m \times d}$, we compute a weighted score matrix $\tilde{S}_{\text{cell}} = [\tilde{s}_{i,j}] \in \mathbb{R}^{m \times d}$ via element-wise multiplication:

$$\tilde{S}_{\text{cell}} = W \odot S_{\text{cell}}.$$

The final row-level anomaly score vector $\boldsymbol{s}_{\text{row}} = [s_{\text{row},1}, \cdots, s_{\text{row},m}]$ is computed by averaging the weighted scores across each row:

$$s_{\text{row},i} = \frac{1}{d} \sum_{j=1}^{d} \tilde{s}_{i,j}, \ \forall i \in \{1, \cdots, m\}.$$

Remarks. Compared to Unweighted Averaging, UWA offers three advantages. (1) It incorporates model confidence into the scoring process, allowing for more informative and introspective anomaly analysis. (2) It naturally downweights unreliable predictions, thereby enhancing robustness against noise and uncertainty. (3) It improves detection performance in scenarios where anomalies affect only a subset of features by emphasizing reliable signals. We validate these benefits through ablation studies in **§5.4**.

4.5 Overall Algorithm

The complete workflow of RFOD is outlined in Algorithm 1. Given a training set X_{train} (assumed to contain only normal samples), a test set X_{test} (which may contain anomalies), and two hyperparameters, α for AGD sensitivity and β for forest pruning, the algorithm outputs both a cell-level anomaly score matrix S_{cell} and a row-level anomaly score vector $\boldsymbol{s}_{\text{row}}$.

Training Phase. For each feature $\boldsymbol{x}^j \in X_{\text{train}}$ ($1 \le j \le d$), RFOD performs a leave-one-feature-out decomposition by treating $\boldsymbol{x}^j$ as the prediction target $\boldsymbol{y}_{\text{train}}^j$ and trains a feature-specific Random Forest RF_j using the rest features $X_{\text{train}}^j = X_{\text{train}} \setminus \{\boldsymbol{x}^j\}$ as input (Line 4). The model type, i.e., classifier or regressor, is selected based on whether the target feature is categorical or numerical (Lines 5–8). To improve generalization and reduce inference overhead, each forest RF_j is then pruned by retaining only the top $\lfloor \beta \cdot t \rfloor$ trees, selected via OOB validation (Line 9).

Inference Phase. During inference, each pruned forest RF_j predicts its corresponding feature $x_{i,j}$ in the test set X_{test}, forming the reconstruction matrix $\hat{X}_{\text{test}}$ and an associated uncertainty matrix U, where each $u_{i,j}$ captures the standard deviation across tree predictions (Lines 10–11). Using the original and reconstructed values, RFOD computes the cell-level anomaly scores S_{cell} via AGD, applied separately to numerical and categorical features as defined in Definitions 4.1 and 4.2 (Line 12). To obtain row-level anomaly scores, the uncertainty matrix U is row-normalized to produce confidence weights W (Lines 13–14), which are then used to reweight S_{cell} and compute the final scores $\boldsymbol{s}_{\text{row}}$ (Lines 15–16).

Time Complexity Analysis. Let t denote the number of decision trees per forest, n the number of training samples, and d the number

---

Algorithm 1: RFOD

Input: Training set $X_{\text{train}} \in \mathbb{R}^{n \times d}$; Test set $X_{\text{test}} \in \mathbb{R}^{m \times d}$;
   Quantile parameter α for Adjusted Gower's Distance (AGD); Retaining ratio β for forest pruning;

Output: Cell-level anomaly score matrix $S_{\text{cell}} \in \mathbb{R}^{m \times d}$;
   Row-level anomaly score vector $\boldsymbol{s}_{\text{row}} \in \mathbb{R}^m$;

1   $\hat{X}_{\text{test}} \leftarrow \mathbf{0}^{m \times d}$;   // Reconstructed test set
2   $U \leftarrow \mathbf{0}^{m \times d}$;   // Uncertainty matrix
3   **for** $j = 1$ **to** d **do**
4     $X_{\text{train}}^j \leftarrow X_{\text{train}} \setminus \{\boldsymbol{x}^j\}$; $\boldsymbol{y}_{\text{train}}^j \leftarrow \boldsymbol{x}^j$;
5   **if** $\boldsymbol{y}_{train}^j$ *is categorical* **then**
6   Train classifier RF_j on $(X_{\text{train}}^j, \boldsymbol{y}_{\text{train}}^j)$;
7   **else**
8   Train regressor RF_j on $(X_{\text{train}}^j, \boldsymbol{y}_{\text{train}}^j)$;
9   Prune RF_j to retain top $\lfloor \beta \cdot t \rfloor$ trees via OOB validation;
10    $\{\hat{\boldsymbol{x}}^j, \boldsymbol{u}^j\} \leftarrow RF_j(X_{\text{test}}^j)$, where $X_{\text{test}}^j \leftarrow X_{\text{test}} \setminus \{\boldsymbol{x}^j\}$;
11    $\hat{X}_{\text{test}}[:, j] \leftarrow \hat{\boldsymbol{x}}^j; U[:, j] \leftarrow \boldsymbol{u}^j$;
12   $S_{\text{cell}} \leftarrow \text{AGD}(X_{\text{test}}, \hat{X}_{\text{test}}, \alpha)$;   // Defs 4.1 and 4.2
13   Normalize each row $\boldsymbol{u}_i \in U$: $\tilde{\boldsymbol{u}}_i \leftarrow \frac{\boldsymbol{u}_i}{\sum_{j=1}^{d} u_{i,j}}, \forall i \in \{1, \ldots, m\}$;
14   Compute confidence weights: $W \leftarrow \mathbf{1}^{m \times d} - \tilde{U}$;
15   $\tilde{S}_{\text{cell}} \leftarrow W \odot S_{\text{cell}}$;   // Element-wise weighting
16   $s_{\text{row},i} \leftarrow \frac{1}{d} \sum_{j=1}^{d} \tilde{s}_{i,j}, \forall i \in \{1, \ldots, m\}$;
17   **return** $S_{\text{cell}}, \boldsymbol{s}_{\text{row}} \leftarrow [s_{\text{row},1}, \cdots, s_{\text{row},m}]$;

---

of features. Each tree has an expected depth of $O(\log n)$ under balanced splits. Training a single random forest for one feature thus incurs a cost of $O(tnd \log n)$. Since RFOD constructs one forest per feature, the overall training complexity is $O(tnd^2 \log n)$.

During inference, each of the m test samples is evaluated across all d forests, each with t trees. As each tree traversal costs $O(\log m)$, the total inference complexity is $O(tmd \log m)$.

Distributed Learning. RFOD is inherently well-suited for distributed computation. The leave-one-feature-out design ensures that each of the d forests can be trained independently, and the t trees within each forest can be trained in parallel. With c compute units available, the td trees can be evenly partitioned, reducing the per-unit training cost to $O\left(\frac{tnd^2 \log n}{c}\right)$.

Inference is even more amenable to fine-grained parallelism. Each prediction of a feature value in a test instance constitutes a lightweight, independent task, yielding a total of mtd atomic tasks, each with a computational complexity of $O(\log m)$. We empirically validate these efficiency gains in **§5.3**.

Summary of Strengths. RFOD brings a range of advantages that make it well-suited for real-world anomaly detection tasks:

- **Label-Free Anomaly Detection:** Requires only normal (non-anomalous) data for training by leveraging a leave-one-feature-out strategy that treats each feature as a pseudo-label, eliminating the need for labeled anomalies.
- **Context-Aware Scoring:** Captures feature-specific conditional dependencies to accurately reconstruct expected values, enabling precise detection of deviations from normal patterns.
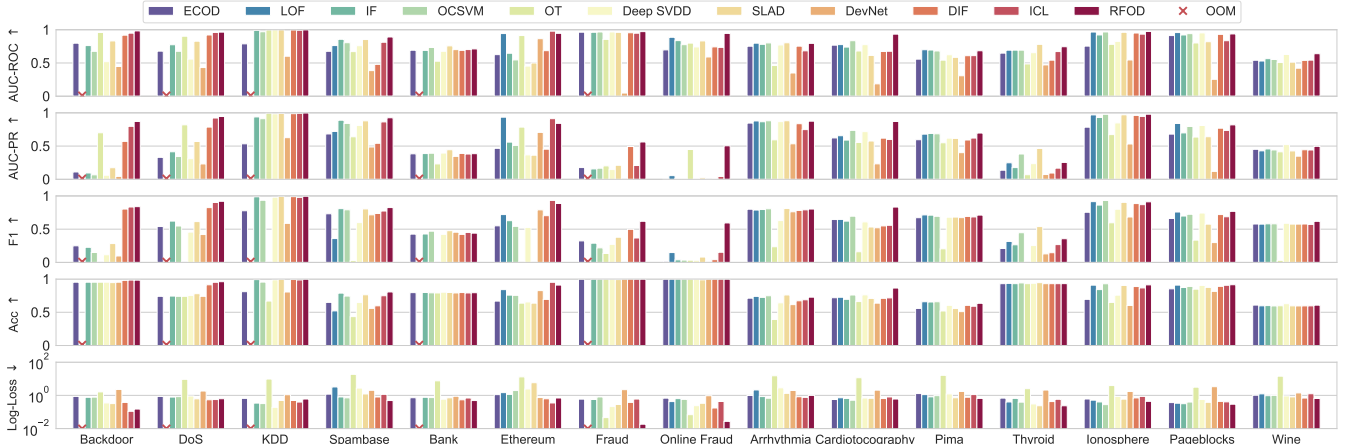
Figure 5: Detection accuracy of all evaluated methods across 15 benchmark tabular datasets.

- **Interpretability:** Generates cell-level anomaly scores that localize abnormal behavior to specific features within a sample, supporting transparent diagnosis and root cause analysis.
- **Scalability:** Naturally supports distributed training and highly parallel inference, allowing the framework to scale efficiently to large, high-dimensional tabular datasets.

5 EXPERIMENTS

We conduct extensive experiments to rigorously assess the effectiveness and practical utility of RFOD across diverse real-world tabular datasets, guided by the following key research questions:

- **Detection Accuracy:** Does RFOD achieve superior detection accuracy compared to state-of-the-art baselines? (**§5.2**)
- **Efficiency:** Can RFOD perform outlier detection in a time-efficient manner suitable for practical use? (**§5.3**)
- **Ablation Study:** How essential are the individual modules of RFOD, such as Forest Pruning, Adjusted Gower's Distance, and Uncertainty Weighting? (**§5.4**)
- **Interpretability:** Do the cell-level and row-level scoring mechanisms of RFOD provide meaningful and actionable explanations for detected anomalies? (**§5.5**)
- **Scalability:** How does RFOD scale with increasing dataset sizes in terms of both accuracy and runtime? (**§5.6**)
- **Parameter Sensitivity:** How sensitive is RFOD to its hyperparameters? (**§5.7**).

We first present the experimental setup, followed by results and analysis for each of the above research questions.

5.1 Experimental Setup

Datasets. We evaluate RFOD on 15 publicly available tabular datasets spanning diverse domains like cybersecurity, finance, and healthcare. Table 3 summarizes key dataset statistics, including sample counts, feature dimensionality, and anomaly ratios. These datasets are widely used in outlier detection research [14, 37, 43], providing robust and comprehensive performance evaluation.

Baselines. We compare RFOD against 10 state-of-the-art methods drawn from both classical data-mining and modern deep-learning paradigms. The data-mining baselines include **ECOD** [29], **LOF**

Table 3: Summary statistics for the 15 benchmark tabular datasets used in our experiments, including sample sizes, feature dimensions, and anomaly ratios.

Domain	Dataset	# Samples	Feature Dim.	Anomaly Ratio
Cybersecurity	Backdoor [34]	95,329	42	2.44%
	DoS [34]	109,353	42	14.95%
	KDD [46]	4,898,430	41	19.86%
	Spambase [26]	4,601	57	39.40%
Finance	Bank [33]	45,211	16	11.70%
	Ethereum [4]	9,841	47	22.14%
	Fraud [19]	284,807	30	0.17%
	Online Fraud	80,000	6	0.14%
Healthcare	Arrhythmia [23]	452	279	45.80%
	Cardiotocography [13]	2,126	22	22.15%
	Pima [45]	768	8	34.90%
	Thyroid [41]	6,916	21	3.61%
Others	Ionosphere [44]	351	34	35.90%
	Pageblocks [32]	5,473	10	10.23%
	Wine [1]	4,898	11	25.38%

[12], **IF** [31], **OCSVM** [51], and **OT** [18]. The deep-learning baselines comprise **Deep SVDD** [42], **SLAD** [53], **DevNet** [38], **DIF** [52], and **ICL** [43].

Evaluation Measures. Following standard evaluation protocols [11, 14, 37, 56], we adopt an unsupervised setting in which 50% of the normal data is used for training. The remaining normal samples are mixed with all anomaly instances to form the test set. Performance is evaluated using:

- **AUC-ROC:** Measures the ranking quality of anomaly scores.
- **AUC-PR:** Emphasizes precision and recall, especially informative under severe class imbalance.
- **F1-Score (F1)** and **Accuracy (Acc):** Threshold-based metrics reflecting classification performance.
- **Log-Loss:** Assesses the calibration of anomaly probabilities.
- **Training Time** and **Testing Time:** Record wall-clock training and testing times to evaluate efficiency and scalability.

Parameter Settings. For all baselines, we adopt hyperparameter settings recommended in their original papers [12, 18, 29, 31, 38, 42, 43, 51–53]. To ensure fair comparisons, we standardize the number of training epochs to 50 for deep models. Moreover, for models that
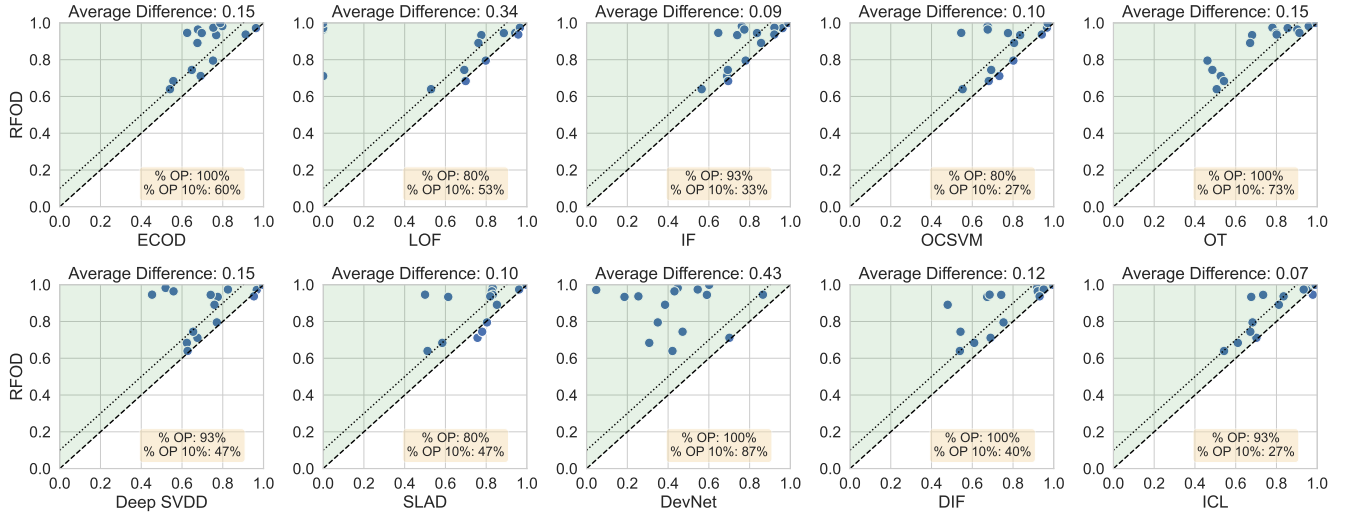
Figure 6: Pairwise comparisons on AUC-ROC between RFOD and other competitors.

require a contamination parameter, we set it equal to the true anomaly ratio in each dataset. Additionally, for Deep SVDD, n_features matches each dataset's feature dimensionality.

Environment. All experiments are conducted on a workstation equipped with an Intel® Xeon® Platinum 8480C @3.80GHz, 256 GB of RAM, and an NVIDIA H200 GPU.

5.2 Detection Accuracy

Main Results. Figure 5 summarizes the performance of all methods across the 15 benchmark datasets. Although RFOD is occasionally outperformed on specific datasets, it consistently secures either the highest or second-highest scores across all metrics and baselines. This reflects not only its strong peak performance but also its overall reliability. In particular, RFOD exhibits substantial improvements in AUC-PR, a critical metric for *imbalanced* outlier detection. Compared to data mining-based methods, RFOD achieves an average AUC-PR gain of 46.7%, and it surpasses deep learning-based approaches by 24.8% in AUC-ROC. These results demonstrate RFOD's capacity to accurately identify true anomalies while maintaining low false positive rates, which is especially crucial in practical scenarios where anomalies are rare yet costly to overlook.

On datasets where RFOD does not rank first, it is outperformed by diverse competitors such as OCSVM, LOF, DIF, and SLAD, rather than by a single consistently superior method. This suggests that no existing alternative uniformly outperforms RFOD, further underscoring its broad applicability across various data characteristics.

Rankings Analysis. Table 4 presents the average rankings of all methods across five evaluation metrics, where lower values indicate better performance. While RFOD might not always achieve first place on every individual dataset, its persistently high rankings highlight its robustness and excellent generalization capabilities. Collectively, these demonstrate that RFOD excels not only in achieving superior performance on specific benchmarks but also in delivering stable, reliable results across diverse scenarios.

Pairwise Comparisons. To provide finer-grained insights, we conduct pairwise comparisons between RFOD and each baseline.

Table 4: Average ranks of all evaluated methods computed over 15 real-world tabular datasets. Lower ranks indicate better overall performance across the benchmarks.

Method	Average Rank ↓				
	AUC-ROC	AUC-PR	F1	Acc	Log-Loss
ECOD [29]	7.40	7.47	7.00	6.77	6.93
LOF [12]	6.00	6.27	6.63	6.50	4.73
IF [31]	5.13	5.73	5.07	5.53	5.47
OCSVM [51]	4.67	5.00	4.47	5.20	5.20
OT [18]	7.53	7.27	10.30	8.83	9.73
Deep SVDD [42]	6.13	6.00	7.13	5.20	6.40
SLAD [53]	5.20	5.07	4.77	6.00	5.20
DevNet [38]	9.93	10.07	8.57	8.77	9.60
DIF [52]	6.53	6.13	5.40	5.60	4.27
ICL [43]	5.67	5.07	4.87	5.27	5.73
RFOD	**1.80**	**1.93**	**1.80**	**2.33**	**2.73**

Figure 6 illustrates scatter plots where each point represents a dataset: the x-axis indicates the AUC-ROC score of the baseline, while the y-axis shows the corresponding score of RFOD. The solid diagonal line represents parity, and dashed lines highlight a +10% margin. Each subplot reports three key metrics: (1) **Average Difference**: Mean absolute difference in AUC-ROC between RFOD and the baseline. (2) **% OP (Outperformed)**: Percentage of datasets where RFOD outperforms the baseline. (3) **% OP 10%**: Percentage of datasets where RFOD exceeds the baseline by at least 10%. These measures provide complementary views on both the magnitude and consistency of performance gains.

RFOD consistently outperforms both data mining and deep learning baselines on most datasets. Compared to data-mining-based approaches, RFOD achieves higher AUC-ROC scores on nearly all benchmarks, with average improvements ranging from 0.07 to 0.43. For example, compared to OT, RFOD secures an average AUC-ROC gain of 0.15, exceeding it by more than 10% on over half the evaluated datasets. Similarly, RFOD demonstrates significant advantages over deep learning methods. Notably, it outperforms DevNet on
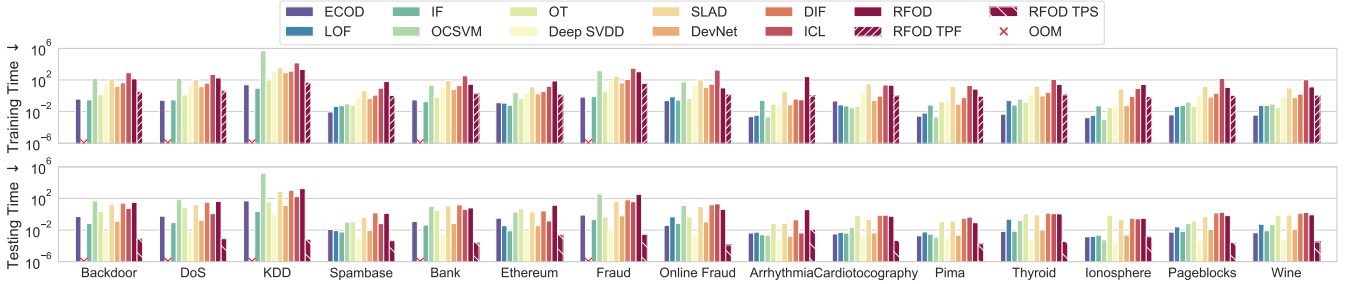
Figure 7: Training and testing time (seconds) of all evaluated methods across 15 benchmark tabular datasets.
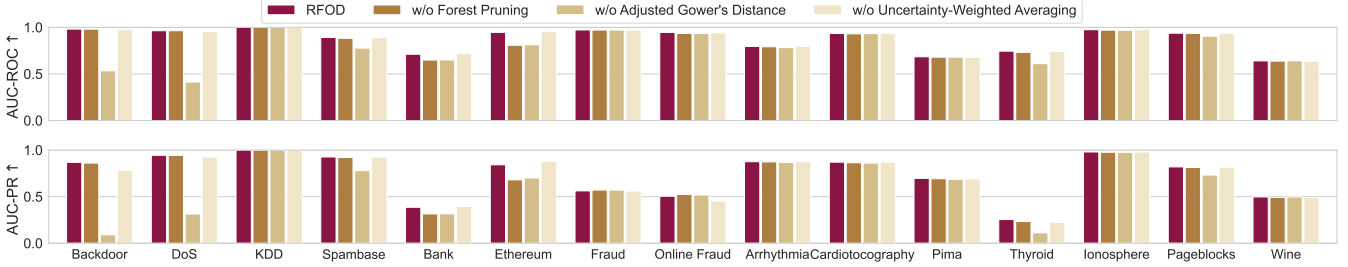

Figure 8: Ablation study results of RFOD on AUC-ROC and AUC-PR across 15 benchmark tabular datasets.

all datasets, achieving an impressive average improvement of 0.43 in AUC-ROC. These gains primarily stem from RFOD's feature-specific modeling and robust handling of mixed-type tabular data, areas where traditional methods often fall short.

5.3 Efficiency

We then evaluate both training and inference times in Figure 7.

Training Time. Data mining-based methods generally exhibit fast training due to their lightweight computations and simple algorithmic designs. However, LOF suffers from out-of-memory errors on large datasets such as DoS and Fraud, highlighting its limited scalability for high-volume data. In contrast, deep learning-based methods are considerably more time-consuming, requiring multiple epochs and significant computational resources, especially for high-dimensional datasets where training time grows substantially.

RFOD strikes a balance between efficiency and performance. While its training time is slightly higher than most data-mining approaches due to training multiple feature-specific forests, it remains significantly faster than deep-learning alternatives. To examine RFOD's internal efficiency, we decompose its training time into the mean Time Per Feature (TPF), shown as hatched bars in Figure 7. Since RFOD trains a separate Random Forest for each feature, TPF offers insight into the per-feature computational cost. Results show that TPF remains moderate and scalable, indicating that RFOD can effectively support parallel processing, as elaborated in **§4.5**.

Testing Time. Inference times are broadly comparable across all methods on each dataset. Notably, RFOD achieves competitive inference speeds, often surpassing data-mining baselines like OCSVM and IF on larger datasets. This stems from its forest pruning strategy and streamlined prediction traversal. To provide finer detail on RFOD's inference cost, we report the Time Per Sample (TPS) as hatched bars in Figure 7. TPS measures the average time required to compute anomaly scores for a single test sample. The results

show that TPS stays consistently low and stable across datasets, underscoring the practical efficiency of RFOD's inference pipeline.

Summary. Overall, RFOD offers an excellent trade-off between detection accuracy and computational efficiency. During training, its modular architecture facilitates independent construction of feature-specific forests, enabling straightforward parallelization and reduced wall-clock times. At inference, pruning less-informative trees streamlines computation, delivering low-latency predictions even for high-dimensional datasets. Compared to deep-learning baselines, which often incur significant training costs, RFOD presents a practical, resource-efficient solution for large-scale anomaly detection in real-world tabular data scenarios.

5.4 Ablation Study

To quantify the contribution of each core component in RFOD, we perform an ablation study by individually disabling three key modules: (1) Forest Pruning, (2) AGD for cell-level scoring, and (3) UWA for row-level aggregation. Each variant alters only one component while keeping the rest of the architecture intact: **w/o Forest Pruning** retains all trees without OOB-based pruning; **w/o Adjusted Gower's Distance** replaces AGD with standard Gower's Distance for cell-level scoring; and **w/o Uncertainty-Weighted Averaging** uses simple averaging instead of UWA for aggregating cell-level scores. We evaluate these variants on all 15 benchmark datasets, reporting results for AUC-ROC and AUC-PR in Figure 8. Similar trends hold for F1-score, Accuracy, and Log-Loss.

Effect of Forest Pruning. Forest Pruning consistently improves performance by removing low-quality trees based on OOB validation. On datasets such as Bank, Ethereum, and Thyroid, where overfitting is common due to small sample sizes or high dimensionality, pruning yields clear gains in both AUC-ROC and AUC-PR. This selective retention not only reduces computation but also enhances generalization by eliminating noisy decision paths.
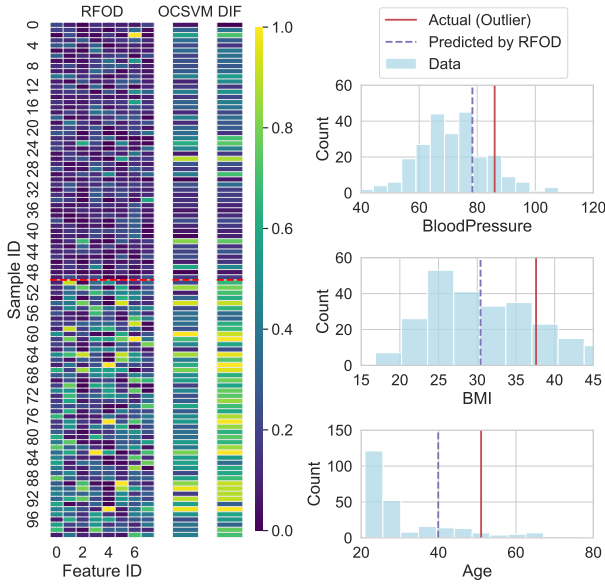
(a) Comparisons of anomaly scoring.   (b) Analysis of one outlier on RFOD.

Figure 9: Case study on Pima (Healthcare).

Effect of Adjusted Gower's Distance. Among all components, AGD proves most critical. Replacing AGD with standard GD results in the steepest performance drops across nearly all datasets. For instance, on the DoS dataset, AUC-ROC plunges from 0.96 to 0.41, a reduction of over 50% in this metric. Similar degradations occur in skewed or heavy-tailed datasets like Spambase, Thyroid, and Page-blocks, underscoring AGD's role in robust scaling and confidence-aware matching for detecting subtle anomalies in mixed-type data.

Effect of Uncertainty-Weighted Averaging. Disabling UWA and using unweighted averaging causes moderate yet consistent performance drops, especially on large datasets like Backdoor and DoS. Without UWA, noisy tree predictions overly influence row-level scores. UWA mitigates this by down-weighting high-variance predictions and amplifying reliable signals, resulting in more stable and precise anomaly rankings.

Summary. Overall, the full RFOD framework, with all components enabled, delivers the highest AUC-ROC and AUC-PR across nearly every dataset. The performance degradation observed when removing any single module confirms the complementary roles of Forest Pruning, AGD, and UWA. These findings validate the architectural choices behind RFOD and demonstrate that its superior performance stems from the synergistic integration of all three components rather than reliance on any individual part.
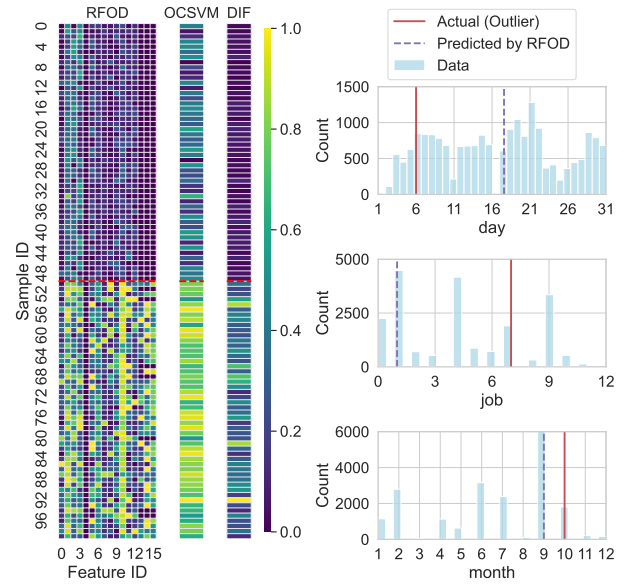
5.5 Case Study

To showcase the interpretability and diagnostic capabilities of RFOD, we present three case studies across healthcare, cybersecurity, and finance, as shown in Figures 9–11. Below, we focus on the Pima dataset from the healthcare domain to provide a detailed walk-through, while similar observations hold for the other datasets.

Comparisons of Cell-Level Anomaly Scores. The Pima dataset consists of 8 physiological features describing patient health profiles. Figure 9(a) displays cell-level anomaly scores for 100 samples across
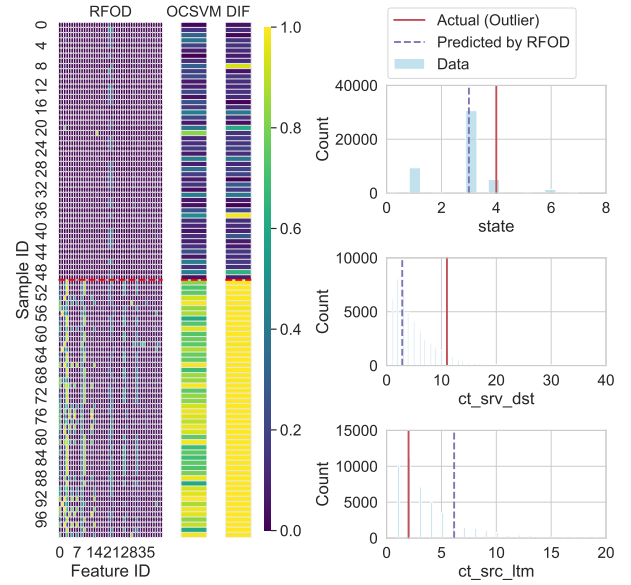
(a) Comparisons of anomaly scoring.   (b) Analysis of one outlier on RFOD.

Figure 10: Case study on DoS (Cybersecurity).

(a) Comparisons of anomaly scoring.   (b) Analysis of one outlier on RFOD.

Figure 11: Case study on Bank (Finance).

these features using RFOD. In this heatmap, darker shades denote lower anomaly scores, while brighter shades highlight potential anomalies, enabling precise, fine-grained insights at the cell level. For comparison, the middle and right heatmaps show results from two strong baselines: OCSVM and DIF. Samples 0–49 represent normal instances, while samples 50–99 are labeled as anomalies. The visualization shows that normal samples under RFOD typically have sparse, low anomaly scores, while anomalies display concentrated high scores in specific features. RFOD highlights distinct feature combinations depending on context, providing targeted
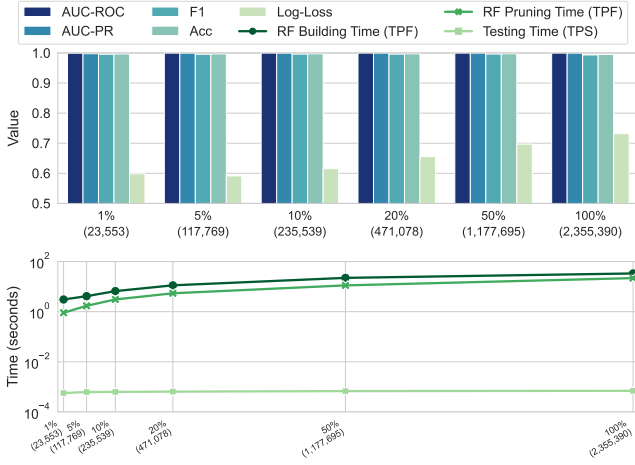
Figure 12: Scalability results on the KDD dataset.

explanations for anomalies. In contrast, OCSVM and DIF often produce uniformly high activation across entire rows or columns, failing to isolate true anomaly sources and generating false positives even for some normal samples.

Row-Level Interpretability. Figure 9(b) illustrates RFOD's row-level interpretability through analysis of a single outlier. It shows feature-wise distributions for `BloodPressure`, `BMI`, and `Age`, with RFOD's predicted values (purple dashed lines) and the outlier's actual values (red solid lines) overlaid. The predicted values fall within high-density regions of the normal distribution, reflecting RFOD's learned expectations, while the actual outlier values lie in the tails, indicating clear anomalies. For instance, the patient's blood pressure and BMI are significantly elevated, while age is unusually low given the context. Such deviations, difficult to spot from marginal histograms alone, are effectively captured by RFOD's conditional modeling.

Summary. Overall, this case study illustrates how RFOD bridges the gap between high detection performance and actionable interpretability. Its cell-level heatmaps facilitate global feature inspection, while per-instance analyses deliver clear, localized explanations. These capabilities are particularly crucial in domains such as healthcare and finance, where understanding the reasons behind an anomaly is as critical as detecting it.

5.6 Scalability

We assess the scalability of RFOD using the largest dataset, KDD, by creating six dataset variants with progressively larger training sets. This evaluation focuses on how detection effectiveness and runtime evolve as the data volume increases.

Effectiveness. The top panel of Figure 12 shows that RFOD consistently achieves high detection performance, even when trained on as little as 1% of the data. This robustness stems from its feature-specific random forests, which effectively model conditional relationships and maintain accuracy under data scarcity.

Efficiency. The bottom panel of Figure 12 breaks down runtime into Random Forest training, pruning, and testing costs. Training time scales roughly linearly with the number of samples, consistent with the complexity analysis in **§4.5**. Notably, testing time remains
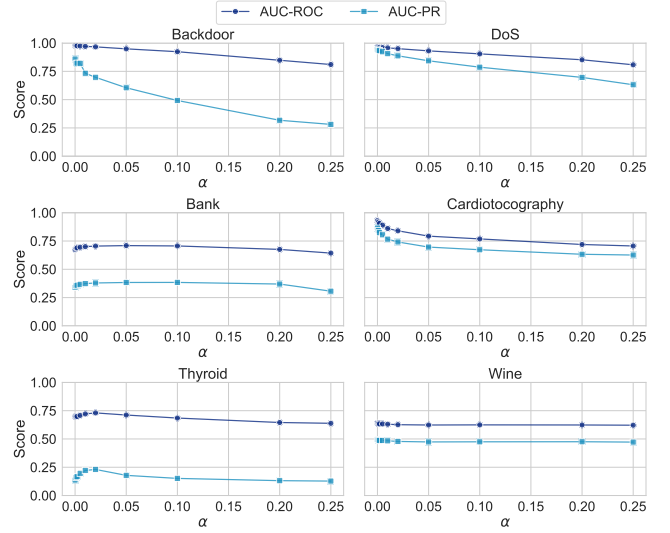

Figure 13: Impact of varying α on six datasets.

low and stable regardless of training size, highlighting RFOD's practicality for large-scale applications.

5.7 Parameter Study

Finally, we examine the sensitivity of RFOD to the hyperparameter α, which controls the distribution tails in AGD for numerical features. We vary α across the set $\{0.001, 0.002, 0.005, 0.01, 0.02, 0.05, 0.1, 0.2, 0.25\}$ and measure AUC-ROC and AUC-PR on six representative datasets covering diverse domains from Table 3. Similar trends are observed across other datasets.

As shown in Figure 13, smaller values of α generally yield higher detection performance. Low α values make AGD more sensitive to subtle deviations by focusing on narrow, high-density regions of the data distribution. However, excessively small α (e.g., below 0.002) can introduce numerical instability due to overly tight quantile ranges, offering limited additional benefit. Based on these results, we recommend selecting α in the range $[0.01, 0.02]$ for most applications, balancing sensitivity and stability.

6 CONCLUSION

This work introduced RFOD, a novel Random Forest–based framework tailored for outlier detection in tabular data. Unlike traditional methods that struggle with heterogeneous features or deep learning approaches that lack interpretability, RFOD reframes anomaly detection as a feature-wise conditional reconstruction task. By training dedicated random forests for each feature and leveraging AGD, RFOD delivers precise, cell-level anomaly scoring that remains robust under skewed distributions and categorical uncertainty. Together with UWA for row-level aggregation and efficient forest pruning, RFOD strikes an effective balance of detection accuracy, scalability, and interpretability. Extensive experiments across 15 real-world datasets show that RFOD consistently outperforms state-of-the-art baselines in both performance and efficiency while delivering actionable insights into the root causes of anomalies. Case studies further demonstrate its practical value in high-stakes domains, highlighting both global and local interpretability.

REFERENCES

[1] Stefan Aeberhard and M. Forina. 1992. Wine. UCI Machine Learning Repository.

[2] Charu Aggarwal. 2017. *Outlier Analysis*. Springer International Publishing.

[3] Haleh Akrami, Anand A Joshi, Jian Li, Sergül Aydöre, and Richard M Leahy. 2022. A robust variational autoencoder using beta divergence. *Knowledge-based systems* 238 (2022), 107886.

[4] Vagif Aliyev. 2020. Ethereum Fraud Detection Dataset. https://www.kaggle.com/datasets/vagifa/ethereum-frauddetection-dataset.

[5] Yihao Ang, Qiang Huang, Yifan Bao, Anthony KH Tung, and Zhiyong Huang. 2023. TSGBench: Time Series Generation Benchmark. *Proceedings of the VLDB Endowment* 17, 3 (2023), 305–318.

[6] Yihao Ang, Qiang Huang, Anthony KH Tung, and Zhiyong Huang. 2023. A Stitch in Time Saves Nine: Enabling Early Anomaly Detection with Correlation Analysis. In *ICDE*. 1832–1845.

[7] Yihao Ang, Qiang Huang, Anthony KH Tung, and Zhiyong Huang. 2024. EADS: An Early Anomaly Detection System for Sensor-Based Multivariate Time Series. In *ICDE*. 5433–5436.

[8] Yihao Ang, Qiang Wang, Qiang Huang, Yifan Bao, Xinyu Xi, Anthony KH Tung, Chen Jin, and Zhiyong Huang. 2025. CTBench: Cryptocurrency Time Series Generation Benchmark. *arXiv preprint arXiv:2508.02758* (2025).

[9] Tharindu R Bandaragoda, Kai Ming Ting, David Albrecht, Fei Tony Liu, Ye Zhu, and Jonathan R Wells. 2018. Isolation-based anomaly detection using nearest-neighbor ensembles. *Computational Intelligence* 34, 4 (2018), 968–998.

[10] Yifan Bao, Yihao Ang, Qiang Huang, Anthony KH Tung, and Zhiyong Huang. 2024. Towards controllable time series generation. *arXiv preprint arXiv:2403.03698* (2024).

[11] Liron Bergman and Yedid Hoshen. 2020. Classification-Based Anomaly Detection for General Data. In *ICLR*.

[12] Markus M Breunig, Hans-Peter Kriegel, Raymond T Ng, and Jörg Sander. 2000. LOF: Identifying Density-Based Local Outliers. In *SIGMOD*. 93–104.

[13] D. Campos and J. Bernardes. 2000. Cardiotocography. UCI Machine Learning Repository. DOI: https://doi.org/10.24432/C51S4N.

[14] Guilherme O Campos, Arthur Zimek, Jörg Sander, Ricardo JGB Campello, Barbora Micenková, Erich Schubert, Ira Assent, and Michael E Houle. 2016. On the evaluation of unsupervised outlier detection: measures, datasets, and an empirical study. *Data Mining and Knowledge Discovery (DMKD)* 30 (2016), 891–927.

[15] Bokai Cao, Mia Mao, Siim Viidu, and Philip Yu. 2018. Collective fraud detection capturing inter-transaction dependency. In *KDD 2017 Workshop on Anomaly Detection in Finance*. 66–75.

[16] Raghavendra Chalapathy and Sanjay Chawla. 2019. Deep Learning for Anomaly Detection: A Survey. *arXiv preprint arXiv:1901.03407* (2019).

[17] Varun Chandola, Arindam Banerjee, and Vipin Kumar. 2009. Anomaly detection: A survey. *ACM Computing Surveys (CSUR)* 41, 3 (2009), 1–58.

[18] David Cortes. 2020. Explainable outlier detection through decision tree conditioning. *arXiv preprint arXiv:2001.00636* (2020).

[19] Andrea Dal Pozzolo, Olivier Caelen, Reid A Johnson, and Gianluca Bontempi. 2015. Calibrating probability with undersampling for unbalanced classification. In *2015 IEEE Symposium on Computational Intelligence and Data Mining (CIDM)*. 159–166. https://www.kaggle.com/datasets/mlg-ulb/creditcardfraud

[20] Marcello D'Orazio. 2021. Distances with mixed type variables some modified Gower's coefficients.

[21] Markus Goldstein and Andreas Dengel. 2012. Histogram-Based Outlier Score (HBOS): A Fast Unsupervised Anomaly Detection Algorithm. *KI-2012: Poster and Demo Track* 1 (2012), 59–63.

[22] John C Gower. 1971. A general coefficient of similarity and some of its properties. *Biometrics* 27 (1971), 857–971.

[23] H. Guvenir, Burak Acar, Haldun Muderrisoglu, and R. Quinlan. 1997. Arrhythmia. UCI Machine Learning Repository.

[24] Songqiao Han, Xiyang Hu, Hailiang Huang, Minqi Jiang, and Yue Zhao. 2022. ADBench: Anomaly Detection Benchmark. In *NeurIPS*. 32142–32159.

[25] Johanna Hardin and David M Rocke. 2004. Outlier detection in the multiple cluster setting using the minimum covariance determinant estimator. *Computational Statistics & Data Analysis* 44, 4 (2004), 625–638.

[26] Mark Hopkins, Erik Reeber, George Forman, and Jaap Suermondt. 1999. Spambase. UCI Machine Learning Repository.

[27] Hans-Peter Kriegel, Matthias Schubert, and Arthur Zimek. 2008. Angle-Based Outlier Detection in High-Dimensional Data. In *KDD*. 444–452.

[28] Zheng Li, Yue Zhao, Nicola Botta, Cezar Ionescu, and Xiyang Hu. 2020. COPOD: Copula-Based Outlier Detection. In *ICDM*. 1118–1123.

[29] Zheng Li, Yue Zhao, Xiyang Hu, Nicola Botta, Cezar Ionescu, and George H Chen. 2022. ECOD: Unsupervised Outlier Detection Using Empirical Cumulative Distribution Functions. *TKDE* 34, 5 (2022), 1454–1495.

[30] Boyang Liu, Ding Wang, Kaixiang Lin, Pang-Ning Tan, and Jiayu Zhou. 2021. RCA: A Deep Collaborative Autoencoder Approach for Anomaly Detection. In *IJCAI*. 1505–1511.

[31] Fei Tony Liu, Kai Ming Ting, and Zhi-Hua Zhou. 2008. Isolation Forest. In *ICDM*. 413–422.

[32] Donato Malerba. 1994. Page Blocks Classification. UCI Machine Learning Repository. DOI: https://doi.org/10.24432/C5J590.

[33] S. Moro, P. Rita, and P. Cortez. 2014. Bank Marketing. UCI Machine Learning Repository. DOI: https://doi.org/10.24432/C5K306.

[34] Nour Moustafa and Jill Slay. 2015. UNSW-NB15: a comprehensive data set for network intrusion detection systems (UNSW-NB15 network data set). In *2015 military communications and information systems conference (MilCIS)*. 1–6.

[35] Nour Moustafa and Jill Slay. 2016. The evaluation of Network Anomaly Detection Systems: Statistical analysis of the UNSW-NB15 data set and the comparison with the KDD99 data set. *Information Security Journal: A Global Perspective* 25, 1-3 (2016), 18–31.

[36] Guansong Pang, Longbing Cao, Ling Chen, and Huan Liu. 2018. Learning representations of ultrahigh-dimensional data for random distance-based outlier detection. In *KDD*. 2041–2050.

[37] Guansong Pang, Chunhua Shen, Longbing Cao, and Anton Van Den Hengel. 2021. Deep learning for anomaly detection: A review. *ACM Computing Surveys (CSUR)* 54, 2 (2021), 1–38.

[38] Guansong Pang, Chunhua Shen, and Anton van den Hengel. 2019. Deep anomaly detection with deviation networks. In *KDD*. 353–362.

[39] Tomáš Pevný. 2016. Loda: Lightweight on-Line Detector of Anomalies. *Machine Learning* 102, 2 (2016), 275–304.

[40] Chen Qiu, Timo Pfrommer, Marius Kloft, Stephan Mandt, and Maja Rudolph. 2021. Neural transformation learning for deep anomaly detection beyond images. In *ICML*. 8703–8714.

[41] Ross Quinlan. 1986. Thyroid Disease. UCI Machine Learning Repository.

[42] Lukas Ruff, Robert Vandermeulen, Nico Goernitz, Lucas Deecke, Shoaib Ahmed Siddiqui, Alexander Binder, Emmanuel Müller, and Marius Kloft. 2018. Deep one-class classification. In *International Conference on Machine Learning (ICML)*. 4393–4402.

[43] Tom Shenkar and Lior Wolf. 2022. Anomaly Detection for Tabular Data with Internal Contrastive Learning. In *ICLR*.

[44] V. Sigillito, S. Wing, L. Hutton, and K. Baker. 1989. Ionosphere. UCI Machine Learning Repository.

[45] Jack W Smith, James E Everhart, William C Dickson, William C Knowler, and Robert Scott Johannes. 1988. Using the ADAP learning algorithm to forecast the onset of diabetes mellitus. In *Proceedings of the Annual Symposium on Computer Applications and Medical Care*. 261–265.

[46] Salvatore Stolfo, Wei Fan, Wenke Lee, Andreas Prodromidis, and Philip Chan. 1999. KDD Cup 1999 Data. UCI Machine Learning Repository. DOI: https://doi.org/10.24432/C51C7N.

[47] Yue Sun, Rick S Blum, and Parv Venkitasubramaniam. 2025. Unifying Explainable Anomaly Detection and Root Cause Analysis in Dynamical Systems. *arXiv preprint arXiv:2502.12086* (2025).

[48] Jianrong Tao, Jianshi Lin, Shize Zhang, Sha Zhao, Runze Wu, Changjie Fan, and Peng Cui. 2019. Mvan: Multi-view attention networks for real money trading detection in online games. In *KDD*. 2536–2546.

[49] David MJ Tax and Robert PW Duin. 2004. Support Vector Data Description. *Machine Learning* 54 (2004), 45–66.

[50] Hu Wang, Guansong Pang, Chunhua Shen, and Congbo Ma. 2021. Unsupervised representation learning by predicting random distances. In *IJCAI*. 2950–2956.

[51] Xuan Wang and Youlu Xing. 2019. An online support vector machine for the open-ended environment. *Expert Systems with Applications* 120 (2019), 72–86.

[52] Hongzuo Xu, Guansong Pang, Yijie Wang, and Yongjun Wang. 2023. Deep isolation forest for anomaly detection. *IEEE Transactions on Knowledge and Data Engineering (TKDE)* 35, 12 (2023), 12591–12604.

[53] Hongzuo Xu, Yijie Wang, Juhui Wei, Songlei Jian, Yizhou Li, and Ning Liu. 2023. Fascinating supervisory signals and where to find them: Deep anomaly detection with scale learning. In *International Conference on Machine Learning (ICML)*. 38655–38673.

[54] Yue Zhao, Xiyang Hu, Cheng Cheng, Cong Wang, Changlin Wan, Wen Wang, Jianing Yang, Haoping Bai, Zheng Li, Cao Xiao, et al. 2021. SUOD: Accelerating Large-Scale Unsupervised Heterogeneous Outlier Detection. *Proceedings of Machine Learning and Systems* 3 (2021), 463–478.

[55] Yue Zhao, Zain Nasrullah, Maciej K Hryniewicki, and Zheng Li. 2019. LSCP: Locally selective combination in parallel outlier ensembles. In *SDM*. 585–593.

[56] Bo Zong, Qi Song, Martin Renqiang Min, Wei Cheng, Cristian Lumezanu, Daeki Cho, and Haifeng Chen. 2018. Deep Autoencoding Gaussian Mixture Model for Unsupervised Anomaly Detection. In *ICLR*.